Applied Catalysis A, General 594 (2020) 117467

Contents lists available at ScienceDirect

Applied Catalysis A, General

journal homepage: www.elsevier.com/locate/apcata

Phosgene formation via carbon monoxide and dichlorine reaction over an activated carbon catalyst: Reaction testing arrangements

Giovanni E. Rossi[a], John M. Winfield[a], Christopher J. Mitchell[b], Willem van der Borden[c], Klaas van der Velde[c], Robert H. Carr[d], David Lennon[a,*]

[a] School of Chemistry, Joseph Black Building, University of Glasgow, Glasgow, G12 8QQ, UK
[b] SABIC UK Petrochemicals Ltd., The Wilton Centre, Wilton, Redcar, TS10 4RF, UK
[c] Huntsman Holland, Merseyweg 10, Botlek Rotterdam, 3197 KG, Netherlands
[d] Huntsman Polyurethanes, Everslaan 45, 3078, Everberg, Belgium

ARTICLE INFO

Keywords:
Phosgene synthesis
Activated carbon
Experimental arrangements
IR spectroscopy
UV-visible spectroscopy

ABSTRACT

An apparatus is described to investigate the synthesis of phosgene from the reaction of carbon monoxide and dichlorine over an activated carbon catalyst. Infrared spectroscopy and UV–vis absorption spectroscopy are used to identify and quantify reagents and products. The reaction is operated with an excess of CO in order to enable complete chlorine conversion at elevated temperatures. The reaction profile is examined over the temperature range of 300 − 445 K, with a phosgene selectivity of 100 % observed at all temperatures. An isosbestic point in the UV–vis spectrum is observed at 272 nm, indicating that the dichlorine and the phosgene are in equilibrium. Examination of the phosgene formation rate as a function of space time and catalyst size fraction at 323 K establishes that, under the described conditions, the reaction is operating under chemical control in the absence of mass transfer restrictions.

1. Introduction

Phosgene is an important intermediate used in the industrial manufacture of polyurethanes, polycarbonates, pharmaceuticals and agrochemicals [1]. It is industrially manufactured *via* the gas phase reaction between carbon monoxide and dichlorine over an activated carbon catalyst [2].

The reaction is strongly exothermic ($\Delta H = -107.6\ kJ\ mol^{-1}$). In industrial operation, the process is operated typically with an excess of carbon monoxide and achieves essentially complete dichlorine conversion, with residual dichlorine levels being less than 100 ppm. Although reaction commences at 30–60 °C, peak reaction temperatures can exceed 500 °C [3].

Despite wide industrial applications, there are relatively few academic laboratory-based studies of catalytic phosgene synthesis catalysis in the literature. The knowledge of handling and analysing this corrosive and hazardous reaction system is primarily retained within a small number of industrial organisations. Representative examples of the relatively few bodies of work accessible in the open literature are considered below. In 1951 Potter and Baron studied phosgene synthesis over an activated carbon catalyst [4] and applied Langmuir-Hinshelwood rate expressions to account for the observed trends. During the period 1977–1980, Shapatina and co-workers examined phosgene reaction kinetics using different commercial catalysts, again adopting Langmuir-Hinshelwood expressions [5–7]. More recently, Gupta et al. examined phosgene synthesis over fullerene (C_{60}) at 473 K [8,9]. On the basis of a combination of experimental measurements and density functional theory (DFT) calculations, the reaction mechanism was reported to conform to a two-step Eley-Rideal-type mechanism; an outcome that is contradictory to the earlier literature for this process. Thus, despite the relevance of phosgene synthesis catalysis to a number of chemical manufacturing stages [1], there is a lack of consensus on the reaction mechanism for this reaction.

Mitchell and co-workers previously examined a range of activated carbons for their suitability as phosgene synthesis catalysts [3]. Eight commercial grade materials were covered in total. The authors used this data as input for a 2-dimensional model that incorporated heat and mass transfer terms to predict catalyst performance in industrial scale phosgene reactors [3]. Despite this resurgence of interest in phosgene synthesis catalysis, aspects of the surface chemistry of the phosgene synthesis process are not comprehensively understood. In relation to activated carbons, this is partially a consequence of the challenges of investigating such materials by optical spectroscopy. The toxic and corrosive nature of reagents and product add extra complexity to the

* Corresponding author.
E-mail address: David.Lennon@glasgow.ac.uk (D. Lennon).

https://doi.org/10.1016/j.apcata.2020.117467
Received 7 November 2019; Received in revised form 28 January 2020; Accepted 12 February 2020
Available online 13 February 2020

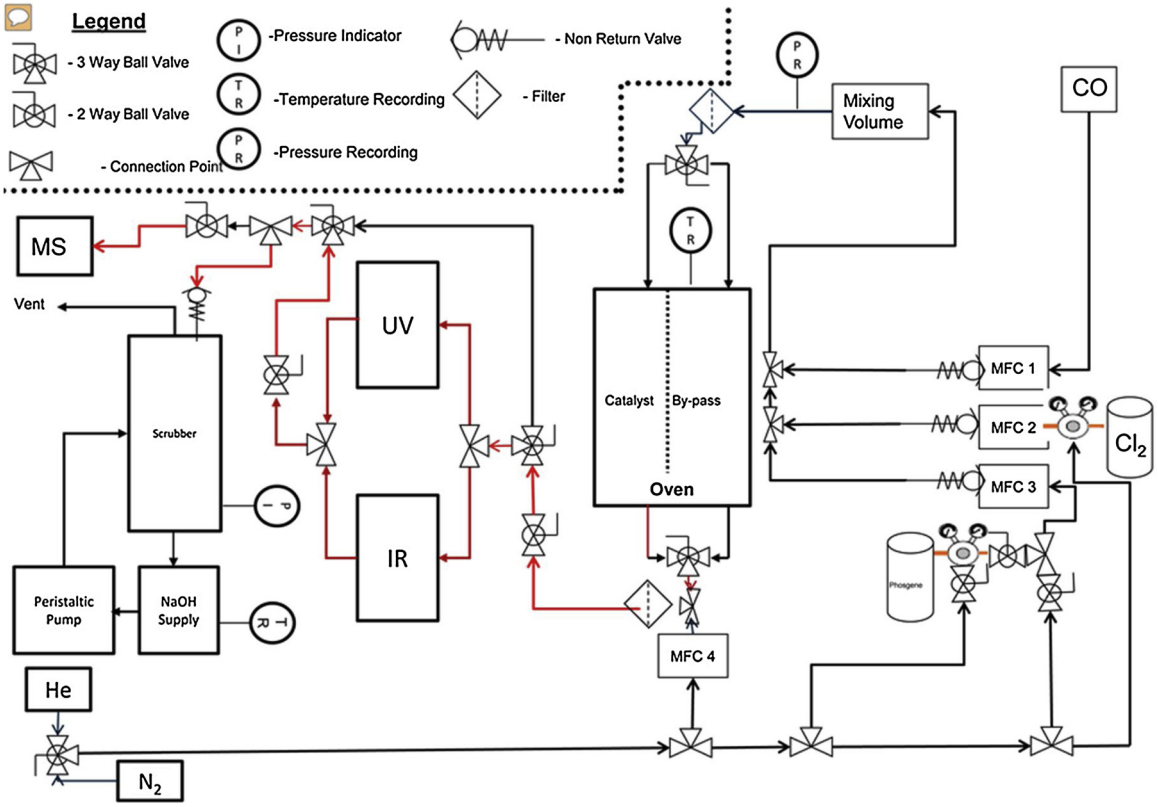

Fig. 1. A schematic representation of the phosgene synthesis catalysis test apparatus.

problem. Just recently, Tüysäuz and co-workers have described a reactor arrangement for investigating issues surrounding phosgene synthesis over activated carbons that utilises in-line spectroscopic analysis to analyse the product stream [10].

Against this background and following on from the broad-ranging studies by Mitchell et al. [3], this work concentrates on investigating reaction trends over a single activated carbon selected from those studied by Mitchell and colleagues: Donau Supersorbon K40. Specifically, the paper describes the development of a reaction test facility constructed within the University of Glasgow's Chemical Process Fundamentals Laboratory that is used to evaluate the reaction kinetics of phosgene synthesis over Donau Supersorbon K40. Whilst the experimental arrangement closely matches that described by Tüysäuz et al. [10] who present preliminary data for the sorption of carbon monoxide and dichlorine over a commercial activated carbon, novel aspects of this work include (i) details of the spectroscopic measurements, (ii) details of safety procedures incorporated in to the experimental protocol, (iii) the consideration of a role for homogeneous chemistry and (iv) an analysis of how phosgene synthesis scales with temperature. The paper is constructed as follows. The test apparatus is comprehensively described in Section 2. Details on the physical characterisation of the catalyst are presented in Section 3.1. Section 3.2 describes how infrared spectroscopy (IR) is used to identify and quantify reagent and product, whilst Section 3.3 does similarly for UV–vis spectroscopy (UV–vis). A role for homogeneous chemistry is considered within Section 3.4. Bringing all these strands together, Section 3.5 presents the reaction profile as a function of temperature. Finally, Section 3.6 explores mass transfer considerations. In this way, the article provides a comprehensive description of a facility that can examine the reaction kinetics of a process involving hazardous and corrosive reagents and products. Although the principal motivation for undertaking this work is directly connected with the large-scale production of phosgene as an integral part of an isocyanate production chain that is associated with the production of polyurethanes, the issues explored are generic and apply to phosgene synthesis in a wide number of applications. Future publications will report on the rate law for phosgene synthesis and on the development of a reaction mechanism for this challenging but industrially relevant reaction system.

2. Experimental

2.1. Catalyst characterisation

All catalytic test measurements were performed on Donau Supersorbon K40 carbon. The catalyst was supplied as pellets (4 mm extrudate) that were ground to a particular size fraction using a manual pestle and mortar and appropriate test sieves (Endcotts). The catalyst was characterised using a number of techniques: X-ray diffraction (XRD), Raman spectroscopy, nitrogen physisorption (BET), and scanning electron microscopy (SEM) accompanied by energy dispersive analysis by X-rays (EDAX). X-ray diffraction measurements were performed on a PAN Analytic X'Pert Diffractometer fitted with a Cu K_α source ($\lambda = 1.5418$ Å) scanning through $85 < 2\theta < 5$ at 0.017 degrees per second. Raman spectra were recorded on a Horiba Jobin Yvon LabRam HR confocal Raman microscope and a 532 nm laser source at < 20 mW power. Brunauer-Emmett-Teller (BET) surface area measurements were performed using a Quantachrome QUADRASORB evo; samples were degassed under argon at 383 K for 16 h prior to nitrogen adsorption. SEM images of the catalyst were obtained using a Philips XL30 ESEM operated at an acceleration voltage of 25 kV. The microscope was additionally equipped with an EDAX facility (Philips/FEI XL30 ESEM) that provided elemental compositional information.

2.2. Phosgene synthesis apparatus

All reactions were performed in the vapour phase. The lines of the apparatus were constructed of stainless steel 1/8″ stainless steel tubing connected by Swagelok fittings throughout (Fig.1). Mass flow

controllers (Hastings HFC-202) connected to Chell 1.04 4-channel display/controller units controlled the flow of incident gases (carbon monoxide: BOC, CP grade; dichlorine: Sigma, purity ≥99.5 %; nitrogen: BOC, 99.998 %; phosgene: BOC, 10 % $COCl_2$ in He) through the reactor with non-return valves positioned after each mass flow controller (MFC). The gas flow control units were operated remotely using Display-X software. The catalyst was contained within a quartz reactor (internal diameter =10 mm) that was connected to the stainless steel gas lines *via* Cajon connectors. The reactor, fitted with a thermocouple pocket, was housed within a temperature controlled oven (Shimadzu GC-14A). On exiting the oven, the reactants were diluted further with nitrogen gas to ensure reagents/products remained in the vapour phase. The exit gases from the reactor were routinely split into two streams that fed in to gas cells located within an infrared spectrometer (Thermo Nicolet Is10) and a UV–vis spectrometer (Shimadzu UV-1800). The IR spectrometer was continually purged with nitrogen (Peak Scientific NitroGen N11LA) to eliminate interference from atmospheric gases. Both spectrometers, housed within individual Perspex boxes that were additionally purged with nitrogen gas, were connected to a PC *via* USB and Ethernet cables to facilitate remote operation. The gas cells were made from Pyrex glass that connected to the stainless-steel gas lines *via* Cajon fittings. The infrared cell utilised KBr windows, whilst the cell for the UV–vis spectrometer used quartz windows. In both cases the windows were sealed to the Pyrex body of the cell by an epoxy adhesive. Under these arrangements the reaction was performed in a dilute regime, where spectroscopic analysis of the regents and products conform to the Beer-Lambert law. Consequently, calibration plots for CO (IR), $COCl_2$ (IR and UV–vis) and Cl_2 (UV–vis) were linear so that, *via* a response factor, quantification of all reactants/products was readily achievable. The applicability of individual calibration plots for CO, $COCl_2$ and Cl_2 to the actual test measurements, where mixtures of gases exist, was tested by passing different combinations of all three gases over ground quartz (reactor by-pass) and determining the associated mass balance. For three variations of gas flows examined, a complete mass balance was returned in all cases. This consistency check indicates that the quantification procedures adopted are applicable to the test scenario. In addition to spectroscopic analysis, a quadrupole mass spectrometer (MKS Spectra Microvision Plus RGA) could also be used to sample the eluting product stream.

The apparatus terminated with a chemical 'scrubber' to clean up the eluting gases. The scrubber was constructed from glass with flexible tubing that was connected to a peristaltic pump (Masterflex, L/S) that circulated a 10 % sodium hydroxide solution so that it was mixed with the exit gas stream. This arrangement ensured no phosgene emission from the apparatus. A thermocouple was placed within the sodium hydroxide solution to detect any heat of reaction that would be associated with a phosgene release. As the apparatus vented to atmosphere, the reaction was run at ambient pressure.

The whole apparatus was located within a walk-in fume cupboard (Premier Laboratory Services), which was equipped with a manually activated high-speed vent facility for activation should any unintended event occur. The laboratory is equipped with two fixed phosgene detectors and one carbon monoxide detector (Crowcon Xgard) mounted adjacent to the fume cupboard that were monitored by a Crowcon Gasmaster control panel. A hand held phosgene and chlorine sensor (Dräger X-AM 5000) was available. Furthermore, operatives wore personal phosgene detection badges (Compur) and personal carbon monoxide detectors (Honeywell gas Alert Clip Extreme). Finally, phosgene detection tape (Honeywell Analytics) was placed at various positions alongside the apparatus as an extra indicator of leaks from the gas lines, or at key points of the control/sensing equipment.

2.3. Catalyst testing

The reactor was typically charged with 125 mg of catalyst of size fraction 250 − 500 μm (Endcotts sieves). The catalyst was placed on a sinter in the middle of the reactor and the reactor inlet was plugged using quartz wool (Sigma). The density of the ground catalyst was 0.805 g ml^{-1}. For activation, the catalyst sample was dried overnight at 383 K in flowing nitrogen (flow rate = 20 ml min^{-1}); this procedure removed any absorbed water. The total flow of the exit gas was kept constant at 159 ml min^{-1}. Standard flow conditions were as follows: 5 ml min^{-1} CO, 4 ml min^{-1} Cl_2, 50 ml min^{-1} N_2 (carrier gas) and 100 ml min^{-1} N_2 (diluent post-reactor), corresponding to a gas hourly space velocity (GHSV) [11] of 22,838 h^{-1}. The initial flow rate (A_0) was determined by passing the gas flow over a by-pass line contained within the oven that contained ground quartz (250 − 500 μm) of comparable volume to the reactor containing catalyst. Once the desired temperature had been attained, the catalyst was exposed to reagents for 20 min before measurements were taken. For variable temperature measurements, 20 min were allowed for the catalyst/reagents to equilibrate thermally before spectroscopic measurements were taken.

Experiments to assess the possibility of mass transport restrictions connected with the above-described experimental arrangements were undertaken by modifying the form of the sample within the reactor. First, whilst retaining the standard size fraction, the possibility of inter-phase mass transfer was examined by varying the catalyst mass in the reactor and the incident flow rate [12]. Second, for a fixed catalyst mass, the size fraction was varied in order to assess a possible contribution from intra-phase mass transfer [12]. These measurements are presented in Section 3.4.

3. Results and discussion

3.1. Catalyst characterisation

Fig. 2 presents the diffraction pattern for the as-received Donau Supersorbon K40 carbon. Apart from a small feature at 2θ = 26° that indicates the presence of a graphitic component; the broad featureless pattern shows the material to be amorphous, with an absence of any long-range order in the material.

The Raman spectrum of the as-received catalyst is shown in Fig. 3(a): the well documented D and G bands of carbonaceous materials at, respectively, 1337 and 1589 cm^{-1} are clearly distinguishable, which are accompanied by weaker overtone and combination features at higher wavenumber. The band at 2671 cm^{-1} is assigned to an overtone of the D band, whilst the 2904 cm^{-1} band is attributed to a combination band from the fundamental D and G modes [14]. The ratio of integrated intensities of the D and G bands (I(D)/I(G)) is 0.90, a value indicative of amorphous sp^2 hybridised carbon [15–17]. Following the approach of Sadezky et al., [18] Fig. 3(b) presents a multi-peak analysis for the Donau Supersorbon K40 carbon, where the cumulative fit of 4

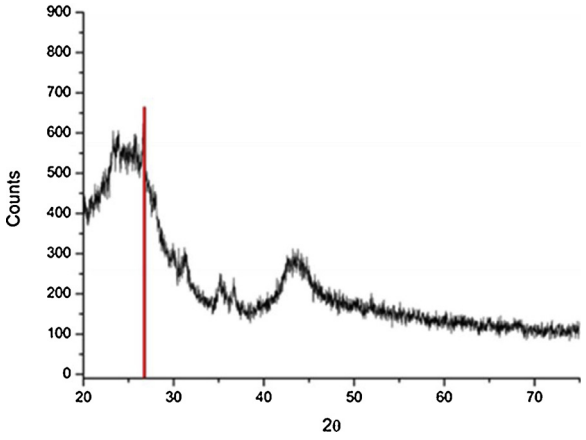

Fig. 2. XRD of the Donau K40 carbon catalyst. The red bar indicates the reflection of graphite [13].

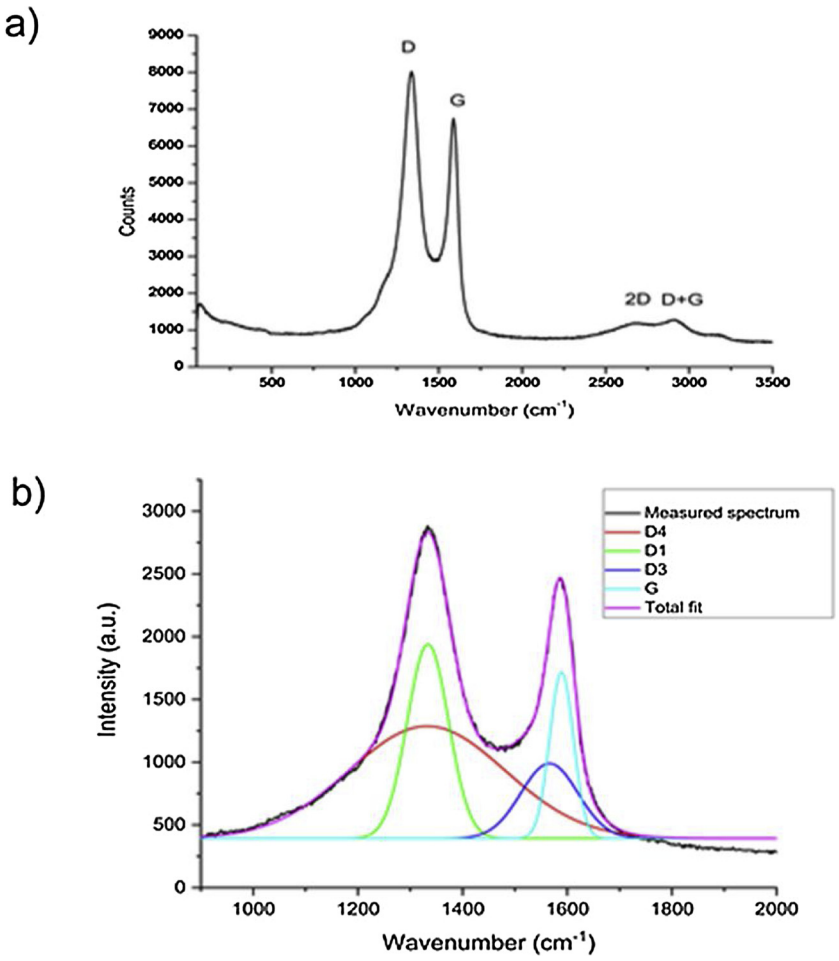

Fig. 3. (a) Raman spectrum of the as-received Donau Supersorbon K40 carbon; (b) Multi-peak fitted Raman spectrum of the Donau Supersorbon K40 carbon.

Table 1
Raman band assignments for Donau Supersorbon K40 carbon [22–24].

Band	Raman Shift (cm^{-1})	Assignment
D4	1180	Disordered graphitic lattice
D1	1350	Disordered graphitic lattice
D3	1568	Amorphous carbon
G	1588	Graphitic lattice

separate peaks is well correlated with the experimental spectrum. Band assignments are outlined in Table 1. The spectrum is indicative of carbonaceous material: disordered carbon (D1, 1348 cm^{-1}; D4, 1182 cm^{-1}), amorphous carbon (D3, 1508 cm^{-1}) and ordered carbon (G, 1601 cm^{-1}) [14,15,19,20]. The presence of the D2 band located at approximately 1620 cm^{-1} is understood to have a positive correlation with the D3 band [21] but has not been fitted here as the peak is difficult to observe [22,23]. Given that XRD shows a minimal presence of graphitic carbon (Fig. 2), the G band at 1601 cm^{-1} is thought to consist of short-range, highly ordered carbon that possesses graphitic-like structure but lacks the long-range order to give rise to an extended network of graphitic carbon.

BET analysis of the as-received catalyst revealed a surface area of 1254 $\pm$ 17 $m^2 g^{-1}$ and a pore volume of 0.579 $\pm$ 0.002 ml g^{-1}, with the errors representing the standard deviation for a set of triplicate measurements. The values are similar to that reported by Mitchell and co-workers [3]. Details on the analysis of the catalyst by scanning electron microscopy are presented in the Supporting Information section. Briefly, Fig. S1 shows the carbon to be composed of a uniform plate-like structure. Fig. S2 shows the EDAX spectrum of the as-received catalyst and Table T1 displays the corresponding elemental analysis, which shows only the presence of carbon and oxygen. Within the detection limits of the instrument (SEM element detection sensitivity > 0.1 %), no residual metal content is associated with the catalyst.

3.2. Infrared spectroscopy

For the case of a reaction system involving a small number of discrete molecules, in-line gas phase infrared spectroscopy represents a convenient way to analyse hazardous gas mixtures. The gas flow arrangements described in Section 2 ensure reagent/product concentrations are dilute, avoiding detector saturation. Infrared spectra were recorded from a total of 32 scans at a resolution of 4 cm^{-1}, corresponding to an acquisition time of ~ 47 s. Fig. 4 presents the infrared spectrum for CO in the carrier stream, with the molecule readily characterised by the C—O stretching mode about 2140 cm^{-1} that is distinguished by P and R rotational branches at 2119 and 2174 cm^{-1} respectively [25]. CO calibration plots were obtained from integration of the ν(CO) band over the region 2260 – 2000 cm^{-1} for carbon monoxide flow rates of 3 – 9 ml min^{-1} in a constant gas flow of 159 ml min^{-1}, nitrogen making up the balance [N_2 (carrier gas) 56 – 50 ml min^{-1}, and N_2 (diluent post-reactor) 100 ml min^{-1}].

Fig. 5 presents the corresponding infrared spectrum for phosgene, which is characterised by two intense bands plus a number of weaker bands. Table 2 confirms the assignments for all of the observed features of the intended product molecule. In a similar fashion to that described for CO, calibration of the phosgene spectral response was achieved *via* integration of the ν_1(CO) mode of phosgene for phosgene flow rates of between 1 – 4 ml min^{-1}. Figs. 4 and 5 demonstrate that the designated

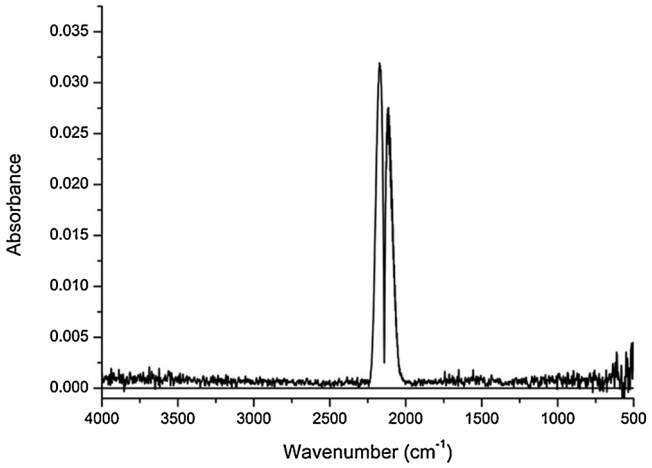

Fig. 4. The infrared spectrum of carbon monoxide flowing through the by-pass reactor at 293 K with a flow rate of CO of 5 ml min^{-1} in a total gas flow rate of 159 ml min^{-1}, *i.e.* 5 ml min^{-1} CO, 154 ml min^{-1} N_2.

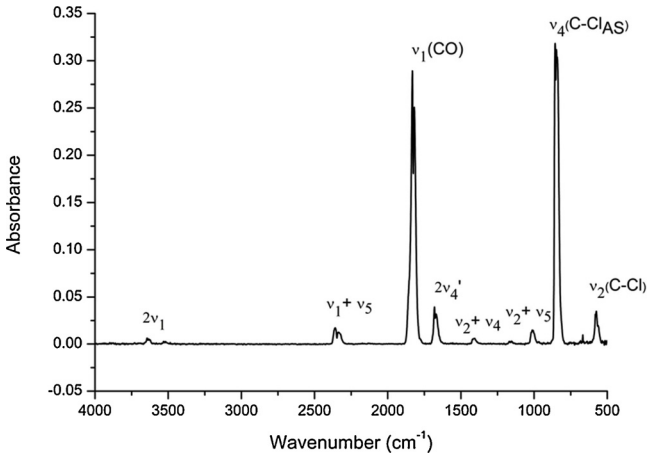

Fig. 5. The infrared spectrum of phosgene flowing through the by-pass reactor at 293 K with a flow rate of $COCl_2$ of 3 ml min^{-1} in a total gas flow rate of 159 ml min^{-1}, *i.e.* 30 ml min^{-1} $COCl_2$/He, 129 ml min^{-1} N_2.

Table 2
Peak assignments for the vibrational spectrum of phosgene [2,25–29].

Peak position cm^{-1}	Assignment
1832, 1820	$\nu_1(a_1)$ ν(CO)
843	$\nu_4(b_1)$ ν(C-Cl)
576	$\nu_2(b_2)$ $\nu(COCl_2)$
3627	$2\nu_1$
2360	$\nu_{1+}\nu_5$
1669	$2\nu_4$'
1402	$\nu_{2+}\nu_4$
1011	$\nu_{2+}\nu_5$

experimental arrangement supports rapid scanning of the eluting gas stream, producing distinct spectra of a respectable signal : noise ratio.

It is worthwhile noting the relevance of assigning all of the bands observed in Fig. 5 and correlated in Table 2. The precision and resolution of the IR measurement provides the opportunity to discern isotopic shifts, as well as being able to identify the influence of impurities that may be present in the feedstream. Such species could exhibit weak features which need to be distinguished from some of the weak phosgene peaks evident in Fig. 5.

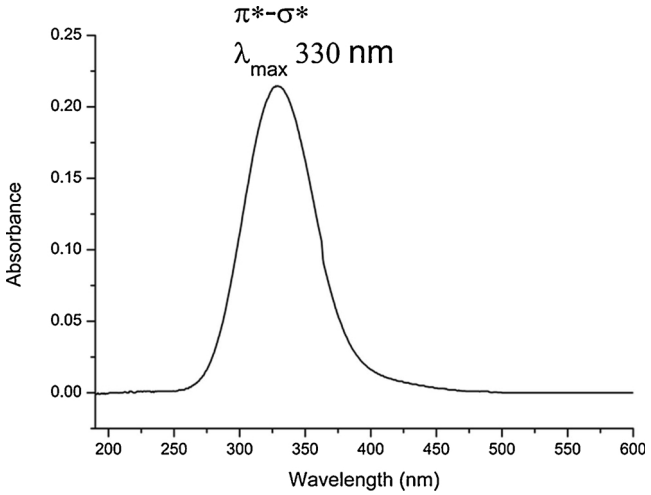

Fig. 6. The UV–vis spectrum of dichlorine flowing through the by-pass reactor at 293 K with a flow rate of Cl_2 of 3 ml min^{-1} in a total gas flow rate of 159 ml min^{-1}, *i.e.* 3 ml min^{-1} Cl_2, 156 ml min^{-1} N_2.

3.3. UV–vis spectroscopy

The primary role for inclusion of a UV–vis spectrometer together with the infrared spectrometer was to identify and quantify dichlorine. Fig. 6 presents a representative spectrum, which is characterised by a broad symmetric band centred at 330 nm that corresponds to the $\pi^* \rightarrow \sigma^*$ transition of dichlorine [30]. The minor glitch observed at about 364 nm is not a spectral feature, rather it corresponds to a grating change in the spectrometer at this wavelength. The integrated peak area between 275 – 474 nm or, alternatively, the peak height at 330 nm was used to calibrate the chlorine spectral response.

Although not its primary role, the UV–vis spectrum can additionally provide information on the degree of phosgene present in the product stream. Fig. 7 shows a spectrum of phosgene passing through the by-pass reactor. Relative to the chlorine spectrum, the band is weak, however the band maximum at 230 nm, attributed to the $\pi \rightarrow \pi^*$ transition of phosgene [25,31], is sufficiently shifted from the chlorine absorption to enable an additional quantification of phosgene formation. The integrated peak area between 214 – 270 nm or, alternatively, the peak height at 230 nm was used to calibrate the phosgene spectral response, providing a useful supplement to the IR phosgene measurements.

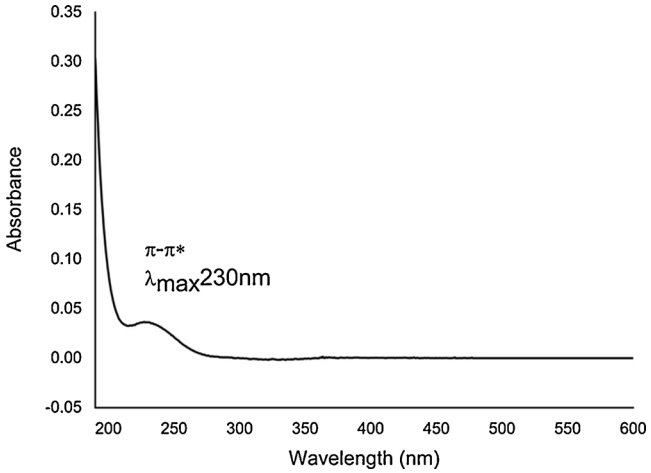

Fig. 7. The UV–vis spectrum of phosgene flowing through the by-pass reactor at 293 K with a flow rate of $COCl_2$ of 3 ml min^{-1} in a total gas flow rate of 159 ml min^{-1}, *i.e.* 30 ml min^{-1} $COCl_2$/ He, 129 ml min^{-1} N_2.

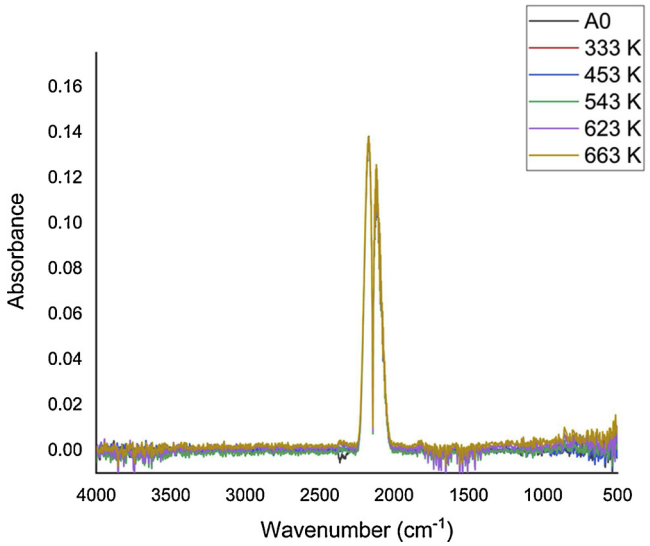

Fig. 8. IR spectra for reaction between CO and Cl_2 over quartz with respective flow rates of 5 ml min^{-1} and 4 ml min^{-1} in a total flow of 159 ml min^{-1} (carrier gas = 50 ml min^{-1} N_2, diluent post-reactor = 100 ml N_2 min^{-1}) over a temperature range of 333-663 K. The A_0 spectrum corresponds to the reaction mixture passing over quartz in the by-pass reactor at 293 K.

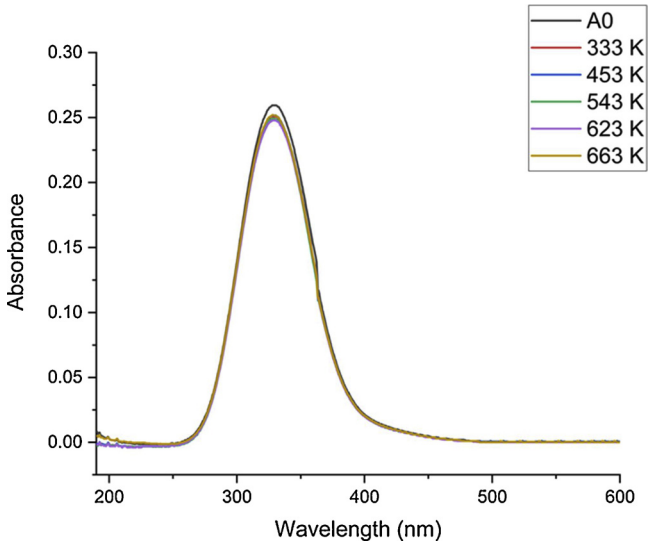

Fig. 9. UV–vis absorption spectra for reaction between CO and Cl_2 over quartz with respective flow rates of 5 ml min^{-1} and 4 ml min^{-1} in a total flow of 159 ml min^{-1} (carrier gas = 50 ml min^{-1} N_2, diluent post-reactor = 100 ml min^{-1} N_2) over a temperature range of 333-663 K. The A_0 spectrum corresponds to the reaction mixture passing over quartz in the by-pass reactor at 293 K.

3.4. Homogeneous processes

Homogeneous chemistry operating alongside heterogeneously catalysed reactions is a possibility for chlorinated reagents operating at elevated temperatures [32,33]. Therefore, in order to assess the prospects of homogeneous contributions to the phosgene synthesis chemistry being explored in the experimental arrangements adopted here (Sections 2.2 and 2.3), a standard reaction mixture of CO and Cl_2 [CO 5 ml min^{-1}, Cl_2 4 ml min^{-1}, carrier gas 50 ml N_2 min^{-1}, diluent post-reactor = 100 ml N_2 min^{-1}; *i.e.* total flow of 159 ml min^{-1}, GHSV = 28,320 h^{-1}] was passed over 125 mg of ground quartz and the reactor output analysed spectroscopically. This corresponds to a space time (τ) of 0.13 s. Fig. 8 presents the FTIR spectrum recorded as the quartz temperature was ramped from ambient (A_0 value) to 663 K. No loss of CO band intensity was observed throughout the full range of temperatures, indicating no CO consumption up to 663 K. Fig. 9 presents the simultaneously recorded set of UV–vis spectra. Here there is some minor variation in peak intensity but it is not systematic and is therefore interpreted as effectively indicating no chlorine consumption during these 'blank' runs. That perception is endorsed in particular by the absence of the phosgene ν(C-Cl) mode at 843 cm^{-1} in Fig. 8 (Section 3.2).

In order to test the homogeneous concept a little further, the space time in the reaction hot zone was increased to 0.25 s by decreasing the carrier gas flow rate to 20 ml N_2 min^{-1} GHSV = 13,920 h^{-1}). This resulted in a minor degree of phosgene formation: 5.0×10^{-3} mmol $COCl_2$ min^{-1} at 663 K (Fig. S3 (IR) and Fig. S4 (UV–vis)). For example, phosgene formation rates over the activated carbon at 400 K are of the order of 1.2 mmol $COCl_2$ $g_{(cat)}{}^{-1}$ min^{-1} (see Section 3.5), *i.e.* even at 263 K above a measured heterogeneous rate of phosgene formation, the homogeneous contribution only amounts to 0.4 % of the heterogeneous rate. Thus, it is concluded that under the standard reaction conditions employed here, there is no homogeneous contribution to the phosgene synthesis process.

3.5. Reaction profile as a function of temperature

The reaction between CO and Cl_2 over Donau Supersorbon K40 was observed as a function of temperature. Adopting a procedure encountered in certain industrial phosgene synthesis facilities, the feed stream of CO and Cl_2 utilised a slight excess of CO [3]; the intention being that all of the Cl_2, can, in principle, be incorporated into the product. The standard reactor gas in-flow [CO 5 ml min^{-1}, Cl_2 4 ml min^{-1}, N_2 (carrier gas) 50 ml min^{-1}] was passed over the by-pass containing ~0.125 g ground quartz until stable signals were detected in the infrared and UV spectrometers; these were taken as the A_0 values for each reagent. The gas flow was then switched over to the catalyst and left for 20 min before spectral acquisition commenced. The temperature was then increased in 20 K steps from 298 − 433 K and the reaction left for 20 min to stabilise before any spectra were recorded.

Fig. 10 presents a sequence of IR spectra obtained as a function of increasing temperature, whilst Fig. 11 presents an equivalent set of UV–vis spectra. Concentrating first on Fig. 10, the A_0 condition for flowing CO and Cl_2 over the by-pass at 293 K yields a spectrum where CO is the only species detected. On switching the reagent feed over the catalyst at 298 K the IR spectrum changes significantly. CO consumption is evident, whilst peaks at 1824 and 843 cm^{-1} are observed that,

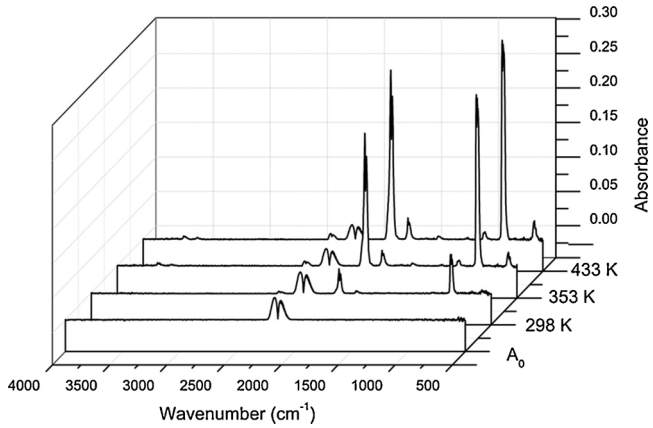

Fig. 10. IR spectra for reaction between CO and Cl_2 over the catalyst as a function of temperature with respective flow rates of 5 ml min^{-1} and 4 ml min^{-1} in a total flow of 159 ml min^{-1} (carrier gas = 50 ml min^{-1} N_2, diluent post-reactor = 100 ml min^{-1} N_2) over a temperature range of 298-433 K. The A_0 spectrum corresponds to the reaction mixture passing over quartz in the by-pass reactor at 293 K.

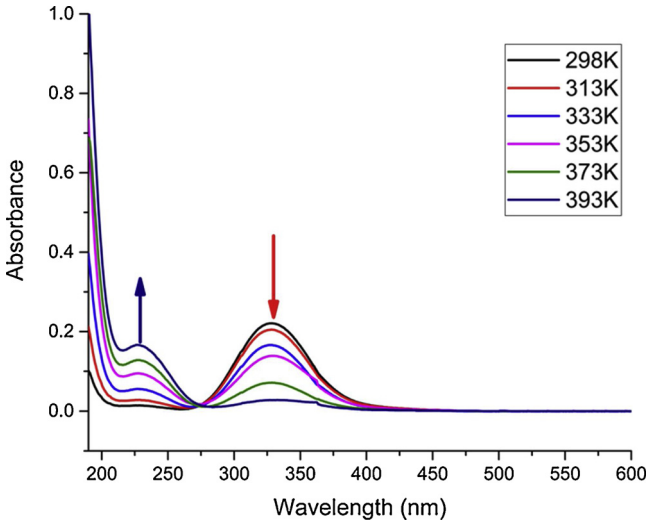

Fig. 11. UV–vis spectra for reaction between CO and Cl_2 over the catalyst as a function of temperature with respective flow rates of 5 ml min^{-1} and 4 ml min^{-1} in a total flow of 159 ml min^{-1} (carrier gas = 50 ml min^{-1} N_2, diluent post-reactor = 100 ml min^{-1} N_2) over a temperature range of 298-433 K.

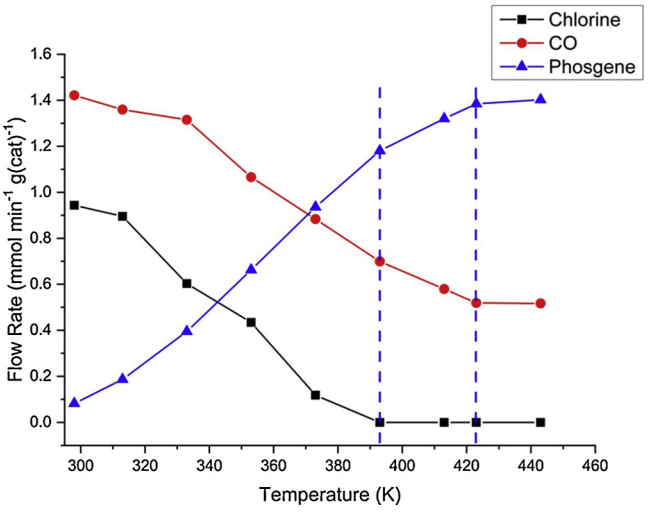

Fig. 12. A plot of CO, Cl_2 and $COCl_2$ flow rates exiting the reactor as CO and Cl_2 are passed over the catalyst over the temperature range 298-445 K. Standard gas flow conditions: 5 ml min^{-1} CO, 4 ml min^{-1} Cl_2, 50 ml min^{-1} N_2 (carrier gas), 100 ml min^{-1} N_2 (diluent post-reactor). The blue dashed line at 393 K signifies complete consumption of dichlorine, whilst the blue line at 423 K signifies the onset of a plateau in the rates of CO consumption and phosgene formation.

with reference to Table 2, may respectively be assigned to the ν_1(CO) and ν_4(C-Cl) modes of phosgene. Increasing the temperature to 353 K simultaneously diminishes the CO bands whilst significantly increasing the phosgene features. Further heating to 433 K leads to more modest changes to the intensity of the CO and $COCl_2$ features.

Two clear trends are evident in the UV–vis spectrum (Fig. 11). First, increasing temperature leads to a systematic decrease in intensity of the dichlorine $\pi^* \rightarrow \sigma^*$ absorption at 330 nm, second there is a concomitant increase in the phosgene $\pi \rightarrow \pi^*$ absorption at 230 nm. An isosbestic point at 272 nm is discernible in Fig. 11. This indicates that the dichlorine and the phosgene are in equilibrium. At 393 K the dichlorine band has virtually disappeared, indicating high conversion of the reagent. No other bands can be distinguished in Fig. 11, indicating Cl_2 and $COCl_2$ to be the only species in the exit stream exhibiting electronic transitions in the 200–500 nm region. Similarly, Fig. 10 shows CO and $COCl_2$ to be the only IR active molecules in the exit stream with absorption in the mid-infrared red region of the spectrum.

Quantification of the spectra presented in Figs. 10 and 11 then leads to the reaction profile as a function of temperature, Fig. 12. Dichlorine conversion progressively increases from 298 K to ~ 390 K, at which point it is completely consumed. CO conversion similarly increases but up to approximately 420 K, thereafter its conversion remains fixed. The comparable form of the decreasing CO and Cl_2 flow rates observed in Fig. 12 is generally reflected in a progressively increasing formation of phosgene up to approximately 420 K when it saturates. It is evident from Fig. 12 that under the stated reaction conditions the reaction is chlorine-limited. Increasing temperature results in increasing conversion of CO and Cl_2 with concomitant formation of $COCl_2$; this trend continues until all of the dichlorine is consumed. However, against that relatively simplistic picture, Fig. 12 hints at additional complexity. Namely, phosgene formation is observed over the range 390 – 420 K, temperatures at which full chlorine conversion is observed. This implies that the incident CO is able to react with chlorine retained by the catalyst to produce phosgene but at temperatures ≥ 420 K no more reactable chlorine is accessible. A better understanding of these important issues of the phosgene synthesis surface chemistry constitutes work in progress. At a temperature of 373 K, a phosgene production rate of 0.48 mmol min^{-1} $g_{(cat)}{}^{-1}$ is observed that corresponds to a specific activity of 3.8×10^{-4} mmol $COCl_2$ min^{-1} $m_{(cat)}{}^{-2}$. Fig. 12 identifies phosgene as the only identifiable product, indicating 100 % selectivity to the desired product under conditions of high reagent conversion.

3.6. Mass transport considerations

Section 3.5 establishes that the selected experimental arrangements can quantitatively speciate reagents and products in this industrially relevant reaction system that involves the reaction and production of hazardous and potentially corrosive materials. It is now appropriate to consider the matter of possible mass transfer restrictions in the measurements. The following section adopts principles laid out by Perego and Paratello [12], in particular catalytic performance is assessed for inter-phase and intra-phase mass transfer contributions.

Experiments were performed where the phosgene formation rate was correlated with reaction space time. Space time (τ) is defined as the quotient of the reactor volume and the volumetric flow rate entering the reactor [12]. Variation of space time was achieved in this instance by fixing the CO and Cl_2 incident flow rates at 5 and 4 ml min^{-1} respectively but selecting carrier gas flow rates of 20, 30 and 50 ml N_2 min^{-1} and then changing the catalyst mass within the range 0.064 – 0.523 g. Fig. 13 shows the resulting plot, which shows a linear correspondence between phosgene production and space time. This condition is indicative that under these conditions the reaction is operating in the absence of inter-phase mass transfer and that the reaction is under chemical (or kinetic) control [12, 34, 35]. It is acknowledged that it is possible that diffusion processes could feature at elevated temperatures.

The possibility of intra-phase mass transport was investigated by examining the phosgene synthesis reaction over a fixed mass of catalyst but selecting a range of size fractions. The catalyst effectiveness factor, η, is the ratio of the activity of the full size catalyst pellets to that obtained on the crushed and sieved catalyst and is an indicator of the presence of internal pore diffusion on catalyst performance [3]. Fig. 14 presents the phosgene formation rate for four distinct size fractions: 180–212, 212–250, 250–500 and 610 – 700 μm. The reaction was performed at 323 K with spectroscopic sampling of the reaction exit stream every 30 min over a 2 h period. All four size fractions return essentially comparable phosgene formation rates, indicating that the catalyst particle size is not affecting the measured reaction rate. This is evidence that the reaction is not experiencing intra-phase mass transfer restrictions and that the reaction is under kinetic control.

The red dashed line in Fig. 14 indicates the phosgene formation rate obtained for the as-supplied catalyst pellets, which shows a significantly

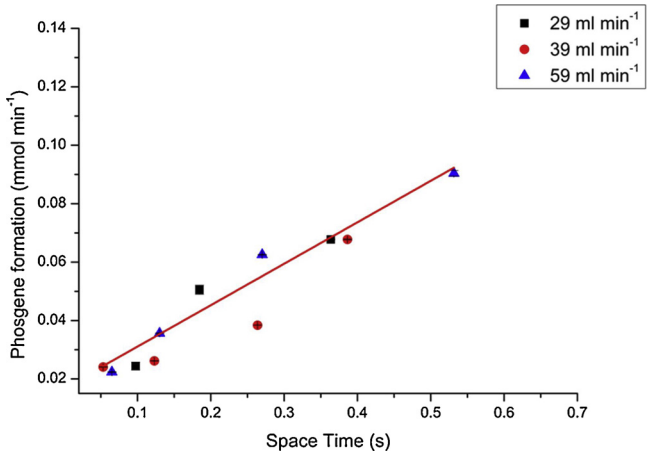

Fig. 13. Phosgene formation rate as a function of space time. CO and Cl_2 incident flow rates fixed at 5 and 4 ml min^{-1} respectively; carrier gas flow rates of 20 (squares), 30 (circles) and 50 (triangles) ml min^{-1} N_2; catalyst mass range = 0.064 – 0.523 g. All measurements were undertaken at a reactor temperature of 323 K.

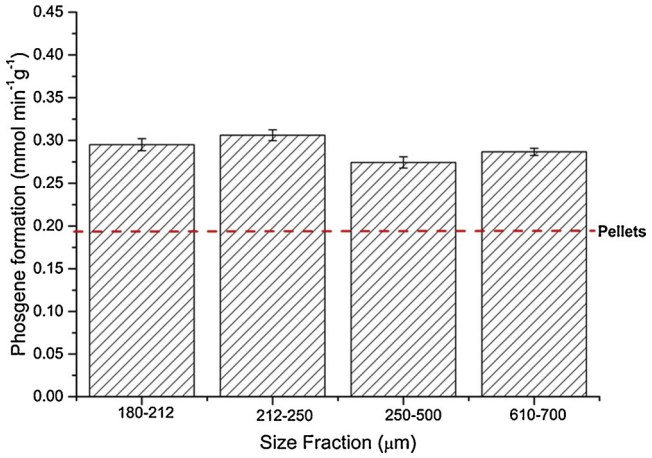

Fig. 14. Phosgene formation rate as a function of catalyst size fraction. Flow rates correspond to steady-state values recorded over a period of 2 h time-on-stream at 323 K. 5 ml min^{-1} CO, 4 ml min^{-1} Cl_2, 50 ml min^{-1} N_2 (carrier gas), 100 ml min^{-1} N_2 (diluent post-reactor). The red dashed line corresponds to the phosgene flow rate determined using as-received catalyst pellets.

reduced synthesis rate when the pellet (0.18 mmol $COCl_2$ min^{-1} $g_{(cat)}{}^{-1}$) is substituted for the powder (0.27 mmol $COCl_2$ min^{-1} $g_{(cat)}{}^{-1}$). This corresponds to an effectiveness factor (η) of 0.70. Mitchell and co-workers report an η value of 0.8 for this catalyst used for phosgene synthesis at 313 K [3].

4. Conclusions

A recently commissioned experimental facility for the reaction testing of a representative phosgene synthesis catalysis (Donau Supersorbon K40 carbon) is described that utilises spectroscopic detection downstream of the reactor to analyse catalyst performance. An IR spectrometer is used to determine the flow rates of CO and $COCl_2$, whilst a UV–vis spectrophotometer determines flow rates for Cl_2 as well as $COCl_2$. Reagent consumption and product formation are followed as a function of temperature and indicate the reaction to be facile at relatively low temperatures (*e.g.* 360 K), with the catalyst affording 100 % selectivity to the desired product. Up to 663 K there is no contribution from homogeneous chemistry. An analysis of mass transport phenomena indicate the reaction testing is undertaken under chemical control. Future work will make use of this apparatus to undertake kinetic and mechanistic investigations of phosgene synthesis over activated carbon catalysts.

CRediT authorship contribution statement

Giovanni E. Rossi: Investigation, Validation, Writing - review & editing, Data curation, Visualization. **John M. Winfield:** Methodology, Investigation, Writing - review & editing. **Christopher J. Mitchell:** Conceptualization, Investigation, Validation, Funding acquisition. **Willem van der Borden:** Methodology. **Klaas van der Velde:** Methodology. **Robert H. Carr:** Conceptualization, Investigation, Funding acquisition, Project administration. **David Lennon:** Conceptualization, Methodology, Investigation, Project administration, Supervision, Writing - original draft, Writing - review & editing.

Acknowledgements

The College of Science and Engineering (GU), the School of Chemistry (GU) and Huntsman Polyurethanes are thanked for project support and the provision of a ph.D. studentship (GER). The EPSRC are additionally thanked for equipment support *via* a Knowledge Exchange award (EP/H500138/1). Dr Claire Wilson and Mr James Gallagher (University of Glasgow) are thanked for technical assistance with, respectively, XRD and SEM measurements.

Appendix A. Supplementary data

Supplementary material related to this article can be found, in the online version, at doi:https://doi.org/10.1016/j.apcata.2020.117467.

References

[1] R. Lin, A.P. Amrute, J. Pérez-Ramírez, Chem. Rev. 117 (2017) 4182–4247.
[2] T.A. Ryan, E.A. Seddon, K.R. Seddon, C. Ryan, Phosgene: And Related Carbonyl Halides, Elsevier Science, 1996.
[3] C.J. Mitchell, W. van der Borden, K. van der Velde, M. Smit, R. Scheringa, K. Ahrika, D.H. Jones, Catal. Sci. Technol. 2 (2012) 2109–2115.
[4] C. Potter, S. Baron, Chem. Eng. Prog. 47 (1951) 473–481.
[5] E.N. Shapatina, V.L. Kuchaeve, M.I. Tempkin, Kinet. Catal. 20 (1978) 972–976.
[6] E.N. Shapatina, V.L. Kuchaeve, M.I. Tempkin, Kinet. Catal. 18 (1977) 968–972.
[7] E.N. Shapatina, V.L. Kuchaeve, B.E. Pen'kovoi, M.I. Tempkin, Kinet. Catal. 17 (1976) 559–566.
[8] N.K. Gupta, A. Pashigreva, E.A. Pidko, E.J.M. Hensen, L. Mleczko, S. Roggan, E.E. Ember, J.A. Lercher, Angewandte Chemie - International Edition (2016) 1728–1732.
[9] N.K. Gupta, B. Peng, G.L. Haller, E.E. Ember, J.A. Lercher, ACS Catal. 6 (2016) 5843–5855.
[10] A. Bähr, G.-H. Moon, J. Diedenhoven, J. Kiecherer, E. Barth, H. Tüysäuz, Chem. Ing. Tech. 90 (2018) 1513.
[11] C.H. Bartholomew, R.J. Farrauto, Fundamentals of Industrial Catalytic Processes, Second Edi, Wiley, 2006, https://doi.org/10.1016/S1351-4180(06)71799-8.
[12] C. Perego, S. Peratello, Catal. Today 52 (1999) 133–145.
[13] K. Sing, Colloids Surf. A Physicochem. Eng. Asp. 187–188 (2001) 3–9.
[14] A.C. Ferrari, D.M. Basko, Nat. Nanotechnol. 8 (2013) 235–246.
[15] A.C. Ferrari, J. Robertson, Phys. Rev. B 61 (2000) 14095–14107.
[16] M. Knauer, M.E. Schuster, D. Su, R. Schlögl, R. Niessner, N.P. Ivleva, J. Phys. Chem. A 113 (2009) 13871–13880.
[17] R. Saito, M. Hofmann, G. Dresselhaus, A. Jorio, M.S. Dresselhaus, Adv. Phys. 60 (2011) 413–550.
[18] A. Sadezky, H. Muckenhuber, H. Grothe, R. Niessner, U. Pöschl, Carbon 43 (2005) 1731–1742.
[19] A.C. Ferrari, J. Robertson, Phys. Rev. B 64 (2001) 1–13 075414.
[20] A.C. Ferrari, J. Robertson, MRS Proceedings, (1999), pp. 299–304 593.
[21] E. Sanchez-Cortezon, M. Dieterle, Y. Uchida, G. Mestl, M. Schur, R. Schlögl, EuroCarbon (2000) Berlin, 9.-13 7. 2000 https://pure.mpg.de/rest/items/item_741748/component/file_741747/content.
[22] J. McGregor, Z. Huang, E.P.J. Parrott, J.A. Zeitler, K.L. Nguyen, J.M. Rawson, A. Carley, T.W. Hansen, J.P. Tessonnier, D.S. Su, D. Teschner, E.M. Vass, A. Knop-Gericke, R. Schlögl, L.F. Gladden, J. Catal. 269 (2010) 329–339.
[23] A.R. McFarlane, I.P. Silverwood, R. Warringham, E.L. Norris, R.M. Ormerod, C.D. Frost, S.F. Parker, D. Lennon, RSC Adv. 3 (2013) 16577–16589.
[24] M.A. Pimenta, G. Dresselhaus, M.S. Dresselhaus, L.G. Cançado, A. Jorio, R. Saito, Phys. Chem. Chem. Phys. 9 (2007) 1276–1290.
[25] G. Hertzberg, Molecular Spectra and Molecular Structure. Part II. Infrared and Raman Spectra of Polyatomic Molecules, Van Nostrand Comp., New York, 1945.
[26] B. Schneider, J. Stokr, Collect. Czech. Chem. Commun. 26 (1961) 1221–1230.

[27] M.J. Hopper, J.W. Russell, J. Overend, J. Chem. Phys. 48 (1968) 3765–3772.
[28] R.J. Jakobsen, Spectrochim. Acta 21 (1965) 433–442.
[29] S. Yamamoto, J. Mol. Spectrosc. 13 (1984) 299–313.
[30] D. Maric, J.P. Burrows, G.K. Moortgat, J. Photochem. Photobiol. A: Chem. 83 (1994) 179–192.
[31] M.R.J. Hachey, F. Grein, Chem. Phys. 224 (1997) 19–31.
[32] I.W. Sutherland, N.G. Hamilton, C.C. Dudman, P. Jones, D. Lennon, J.M. Winfield, Applied Catalysis A: Gen. 399 (2011) 1–11.
[33] I.W. Sutherland, N.G. Hamilton, C.C. Dudman, P. Jones, D. Lennon, J.M. Winfield, Appl. Catal. A Gen. 471 (2014) 149–156.
[34] J.F. Le Page, Applied Heterogeneous Catalysis : Design, Manufacture, Use of Solid Catalysts, Paris : Éditions Technip, 1987.
[35] C.N. Satterfield, Mass Transfer in Heterogeneous Catalysis, M.I.T. Press, 1970.